The corrosion behavior of hafnium in high-temperature water environments

D.M. Rishel *, J.D. Smee, B.F. Kammenzind

Bettis Atomic Power Laboratory, Bechtel ettis, Inc., P.O. Box 79, West Mifflin, PA 15122-0079, USA

Abstract

The high-temperature water corrosion performance of hafnium is evaluated. Corrosion kinetic data are used to develop correlations that are a function of time and temperature. The evaluation is based on corrosion tests conducted in out-of-pile autoclaves and in out-of-flux locations of the Advanced Test Reactor at temperatures ranging from 288 to 360 °C. Similar to the corrosion behavior of unalloyed zirconium, the high-temperature water corrosion response of hafnium exhibits three corrosion regimes: pretransition, post-transition, and spalling. In the pretransition regime, cubic corrosion kinetics are exhibited, whereas in the post-transition regime, linear corrosion kinetics are exhibited. Because of the scatter in the spalling regime data, it is not reasonable to use a best fit of the data to describe spalling regime corrosion. Data are presented to show that in the pretransition regime, neutron irradiation does not alter the corrosion performance of hafnium © 2002 Elsevier Science B.V. All rights reserved.

1. Background

The US Department of Energy has been tasked with the establishment of a long-term disposal capability of spent fuel from nuclear reactors. The primary function of the repository is to ensure that the environment is protected by delaying and controlling the release of radioactive material. Initially, disposal canisters will provide the primary barrier to the release of radioactive material. In addition to the disposal canisters, Zircaloy fuel cladding provides a significant additional barrier for Naval fuel. Hillner et al. [1] recently reported on Zircaloy corrosion based on long-term Zircaloy autoclave corrosion data. These data were used to estimate the amount of corrosion that may be experienced by spent Zircaloy-clad fuel assemblies during long-term exposure to geologic repository conditions.

To ensure adequate reactivity control, hafnium may be inserted into fuel assemblies. In some cases, this hafnium could be irradiated. As is the case for Zircaloy

cladding [1] it is important to understand the corrosion behavior of Hf. Compared to the Zircaloys, there are little hafnium corrosion data in the open literature. Most of the hafnium corrosion data reported have been obtained at temperatures greater than 350 °C in gaseous environments such as oxygen, air, or steam [2–5]. Smeltzer and Simnad [5] systematically determined the reaction kinetics of hafnium in pure dry oxygen. In that study, hafnium crystal bar material containing up to 5.0 w/o Zr was used. Gravimetric measurements were made at an oxygen pressure of 760 mm Hg at temperatures ranging from 350 to 1200 °C.

Smeltzer and Simnad [5] found that the following logarithmic, parabolic, and linear rate equations represented their data for the temperature ranges of 350–710 °C, 470–1200 °C and 900–1,200 °C, using activation energies of 47.6, 150.4, and 109.0 kJ/mol, respectively.

$$\Delta W' = 2 \times 10^{-2} \left(\exp \frac{-47\,630}{RT} \right)$$
$$\ln \left[1 + \left(7.7 \left(\exp \frac{-22\,562}{RT} \right) \right) t \right], \tag{1}$$

---

* Corresponding author.
E-mail address: risheldm@bettis.gov (D.M. Rishel).

$$\left(\Delta W'\right)^2 = \left(6 \times 10^{-2} \exp \frac{-150\,411}{RT}\right)t + a(T) \qquad (2)$$

and

$$\Delta W' = \left(6 \times 10^{-2} \exp \frac{-109\,048}{RT}\right)t + b(T), \qquad (3)$$

where $\Delta W'$ is the oxygen weight gain in units of gm/cm^2, t is the time in minutes, R is the gas constant (in J/mol/K), T is the temperature in K, and a and b are temperature-dependent constants. The logarithmic and parabolic empirical relationships are correlated with the formation of compact oxides, while the linear rate empirical relationship is associated with a layered porous scale. Parabolic oxidation behavior obeys the Wagner theory of oxidation, which for hafnium oxidation occurs with the inward diffusion of oxygen as ions, via anion vacancies, to react with hafnium at the metal/oxide interface [6]. The mechanisms associated with the logarithmic relationship are not as well established but are interpreted to be based on the adsorption of reactive species, the effects of electric fields across oxide layers, quantum-mechanical tunneling of electrons through thin scales, progressive blocking of low-resistance diffusion paths, nonisothermal conditions in the oxide layer, and nucleation and growth processes [6]. The linear rate relationship may reflect a reaction that is controlled by diffusion through a thin inner layer of the oxide that is maintained at a constant thickness with time due to repetitive delamination or exfoliation of hafnium oxide. Alternatively, the linear rate relationship may reflect a rate-determining phase boundary process, e.g., nucleation and growth of the oxide [7].

There are a few reports describing the corrosion response of hafnium under aqueous environments. In these studies the reported information describes the corrosion behavior of hafnium under a specific set of conditions. For example, in Russian WWER-1000 pressurized water reactors, it has been reported [8] that hafnium has been considered for use as neutron absorbing components. Corrosion test results indicate that under conditions corresponding to WWER-1000 primary circuit water, the corrosion resistance of pure hafnium is very high (in WWER-1000 PWRs the inlet and outlet water temperatures are 290 and 320 °C, respectively). Furthermore, under irradiation hafnium was reported to retain its high corrosion resistance. After 26,800 h at operating conditions, a dense oxide film, 5–20 μm thick formed, for which the corrosion rate was essentially zero after the first 4000 h of operation. In Japan, hafnium is one material being used in advanced control rods for BWR plants [9]. One reason for the selection of hafnium is its superior corrosion performance. Corrosion test results in steam at 500 °C and 10.5 MPa found that although hafnium undergoes nodular corrosion, it exhibits supe-

rior corrosion performance to that of Zircaloy-4. The addition of small amounts of iron improved resistance to nodular corrosion [9].

The properties of Shippingport PWR hafnium control rods were reported in Refs. [10,11]. The corrosion film thicknesses formed on the surface of a control rod that had experienced up to 1100 days of exposure (21 035 effective full power hours) at temperatures of approximately 280 °C were found to range in thickness from 0.16 to 0.34 μm [11]. The oxide-film thicknesses of all irradiated hafnium material taken from this control rod were very similar. There were essentially no differences among sections exposed to thermal neutron fluences ranging from 4.5×10^{24} to 7.4×10^{24} n/m^2, and fast neutron (>1 MeV) fluences ranging from 36×10^{24} to 54×10^{24} n/m^2.

The examples cited above suggest that hafnium has a high resistance to corrosion; however, there are little published corrosion data from systematic studies to use in aqueous corrosion rate correlations. The use of the available published kinetic data obtained from elevated temperature experiments conducted in gaseous environments in predicting the corrosion behavior of hafnium at lower temperatures in aqueous environments requires significant extrapolations due to the vastly different environmental conditions. Lower-temperature water corrosion data would reduce the extrapolation. To provide a basis for evaluating the corrosion behavior of hafnium in a repository environment, correlations of hafnium corrosion are developed from corrosion data generated by the Bettis Atomic Power Laboratory in high-temperature water environments. These data were generated from tests that have been conducted over a 25 year period with accumulated exposure times up to 16 years. The results of this analysis are presented below.

2. Experimental

2.1. Specimens

Corrosion tests were conducted on fully annealed and recrystallized specimens fabricated from material that meets or exceeds the chemical composition of ASTM B 776, nuclear grade (R1) hafnium. Corrosion specimens were made from nine different ingots, for which the compositions are listed in Table 1. The corrosion data were obtained with specimens of three different sizes and prefilmed under four different prefilm conditions (see Table 2). Prior to prefilming or testing (in the case for specimens tested without any prefilm), the specimens were pickled to a bright surface finish in a bath comprised of approximately 39 v/o nitric acid, 3 v/o hydrofluoric acid and the balance water. The specimens were pickled long enough to ensure that approximately 50 μm of material was removed per surface.

Table 1
Ingot composition (in wppm unless otherwise indicated)

Element	Ingot A	Ingot B	Ingot C	Ingot D	Ingot E	Ingot F	Ingot G	Ingot H	Ingot I
Hf (wt%)	>95.3	>95.3	>95.3	>95.3	>95.3	>95.3	>95.3	>95.3	97.2–97.6
Fe	82–138	173–186	152–169	139–166	179 190	99–123	131–165	140–175	290–300
O	180–280	170–190	170–190	220–250	170–200	110–253	126–265	220–250	270–370
Al	<50	<50	<50	<50	<50	<50	<50	<50	30–38
C	30	50	<30	40–50	<30	<75	<75	<20	<30
Cu	<50	<50	<50	<50	<50	<50	<50	<25	<40
H	<5	6	7	7	<5	<5	<5	<3	2.7–3.6
Mo	<10	<10	<10	<10	<10	<10	19	<10	10–20
N	22	19–20	24–27	15–23	17	<50	<50	29–38	18–26
Nb	<50	<50	<50	<50	<50	<50	<50	<50	<100
Ta	<100	<100	<100	<100	<100	<100	<100	<100	<200
Ti	<50	<50	<50	<50	<50	<50	<50	<25	33–37
U	0.92	1.12	1.21	0.87	0.84	<2	<2	<1	<0.5
W	<75	<75	<75	<75	<75	<75	<75	<20	<20
Zr (wt%)	2.53–2.61	2.64–2.86	2.77–2.83	3.17–3.23	2.94–3.01	2.5–2.7	2.6–2.8	1.5–1.9	2.35–2.75
B	<0.5	<0.5	<0.5	<0.5	<0.5	<0.5	<0.5	<0.5	Not available
Cd	<2.5	<2.5	<2.5	<2.5	<2.5	<2.5	<2.5	<2.5	
Co	<5	<5	<5	<5	<5	<5	<5	<5	
Cr	<100	<100	<100	<100	<100	<100	<100	<20	
Gd	<2.5	<2.5	<2.5	<2.5	<2.5	<3.5	<3.5	<1	
Mn	<25	<25	<25	<25	<25	<25	<25	<20	
Ni	<25	<25	<25	<25	<25	<25	<25	<25	
P	<3	<3	<3	<3	<3	<10	<10	<3	
Pb	<10	<10	<10	<10	<10	<10	<10	<5	
Si	<25	26	28	<25	35	<25	<25	<25	
Sn	<10	<10	<10	<10	<10	<10	<10	<10	
Th	<3.5	<3.5	<3.5	<3.5	<3.5	<3.5	<3.5	<1	
V	<25	<25	<25	<25	<25	<25	<25	<10	

Table 2
Summary of material and test conditions

Test	Group[a]	No. of specimens	No. of ingots	Temperature (°C)	Prefilm conditions[b]	Test environment	Sample size
1	A	7	7	360	3-day	Autoclave (pH 10)	–[c]
2		2	2 of 7[d]		14-day		
3		2	2 of 7[d]		Anodized		
4		3	3 of 7[d]		No prefilm		
5	B	7	7	360	No prefilm	Autoclave (pH 7)	–[c]
6	C	30	1	360	No prefilm	Autoclave (pH 7)	–[e]
7	D	7	7	354	3-day	ATR Out-of-flux (pH 10)	–[c]
8		2	2 of 7[d]		14-day		
9		2	2 of 7[d]		Anodized		
10		3	3 of 7[d]		No prefilm		
11	E	7	7	338	3-day	Autoclave (pH 10)	–[c]
12		2	2 of 7[d]		14-day		
13		2	2 of 7[d]		Anodized		
14		3	3 of 7[d]		No prefilm		
15	F	7	7	332	3-day	ATR Out-of-flux (pH 10)	–[c]
16		2	2 of 7[d]		14-day		
17		2	2 of 7[d]		Anodized		
18		3	3 of 7[d]		No prefilm		
19	G	7	7	316	3-day	Autoclave (pH 10)	–[c]
20		2	2 of 7[d]		14-day		
21		2	2 of 7[d]		Anodized		
22		3	3 of 7[d]		No prefilm		
23	H	7	7	310	3-day	ATR Out-of-flux (pH 10)	–[c]
24		2	2 of 7[d]		14-day		
25		2	2 of 7[d]		Anodized		
26		3	3 of 7[d]		No prefilm		
27	I	8	1	288	3-day	Autoclave (pH 10)	–[f]

[a] The specimens associated with each of the tests in this group were tested in the same autoclave or ATR loop at the indicated temperature and pH.
[b] Days are in 360 °C, pH 7 water unless where otherwise indicated.
[c] Dimensions (cm): 2.36 × 2.36 × 0.10.
[d] n of the 7 ingots listed in Tests 1, 7, 11, 15, 19 and 23.
[e] Dimensions (cm): 2.54 × 3.81 × 0.51.
[f] Dimensions (cm): 7.62 × 1.91 × 0.05.

2.2. Corrosion tests

Isothermal corrosion tests were conducted either in static autoclaves or in flowing test loops in the Advanced Test Reactor (ATR) in out-of-neutron flux positions. [1] Corrosion data were obtained from fifteen autoclave and twelve ATR tests that included a total of 129 coupons. The autoclave tests were conducted at one of four nominal temperatures; 288, 316, 338, and 360 °C. The ATR tests were conducted at one of three nominal temperatures; 310, 332, and 354 °C. All tests, in both the static autoclaves and ATR, were conducted under sub-

cooled, pressurized water conditions. A summary of the materials and test conditions that were evaluated is provided in Table 2. With two exceptions, all tests were conducted in water in which (1) the room-temperature pH was maintained between 10.1 and 10.3, (2) the oxygen content was less than 20 ppb, (3) the hydrogen content was maintained between 10 and 60 cm^3 H$_2$/kg H$_2$O and (4) the conductivity was maintained between 20 μS/cm to 80 μS/cm. Tests numbered 5 and 6 were conducted in deionized, degassed water, at a room-temperature pH of 7. During the course of the corrosion tests, the corrosion coupons were periodically weighed to determine the corrosion weight gains. Hafnium is such a corrosion resistant material that the magnitudes of weight gain measurements are very small. A weight gain of 1 mg/dm^2 corresponds to a weight increment on the specimen of approximately 0.1 mg, the resolution of measurement balances.

[1] Although other hafnium coupons were exposed to neutron fluxes, corrosion data could not be obtained via weight gain measurements due to the fact that the most significant contributor to the observed weight gain was due to neutron capture.
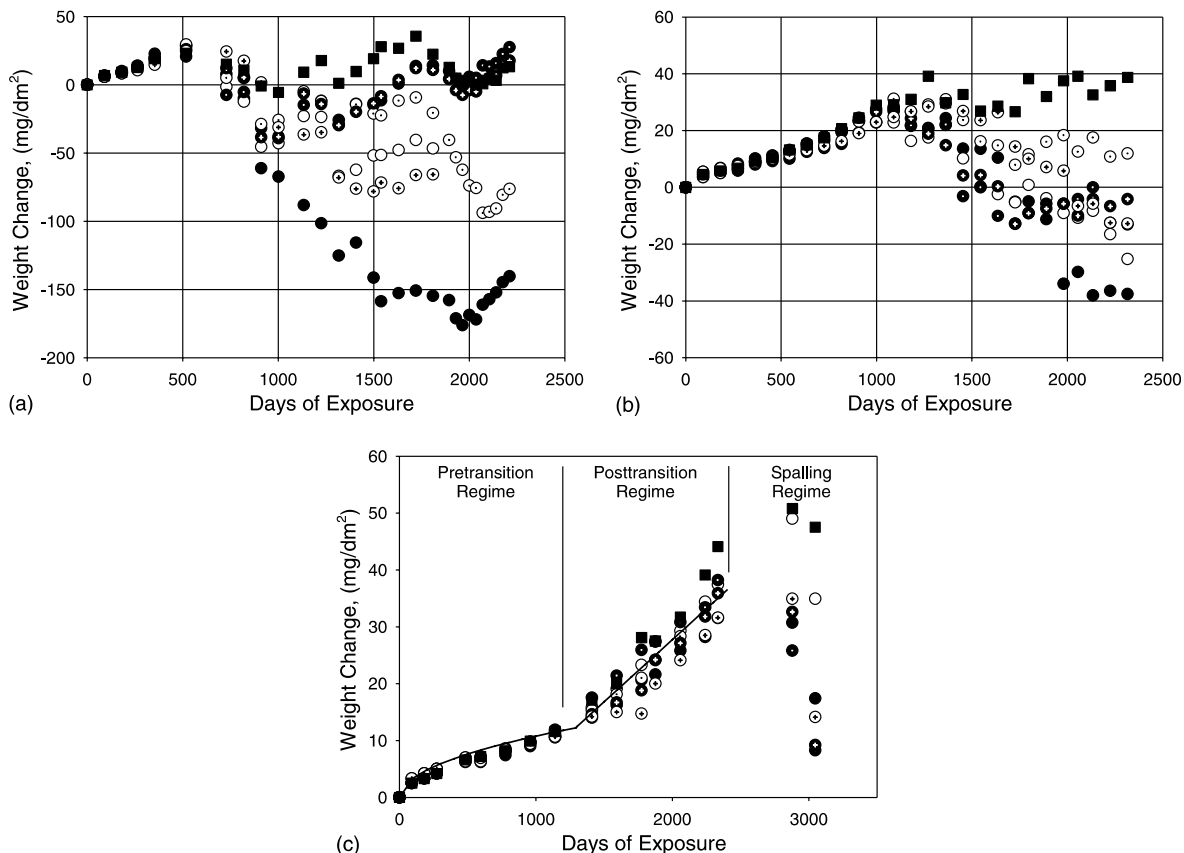
Fig. 1. Weight change behavior of hafnium at: (a) 360 °C (Test 1), (b) 338 °C (Test 11) and (c) 316 °C (Test 19), in water with a room temperature adjusted pH of 10. All coupons had a 3-day 360 °C prefilm applied before the test.

3. Results and model development

3.1. Observed behavior

Hafnium is in the same group in the periodic table as zirconium, and like zirconium it forms only one stable oxide, HfO_2. In water, the formation of the corrosion film, HfO_2, can be described by the following reaction:

$$Hf + 2H_2O = HfO_2 + 2H_2. \qquad (4)$$
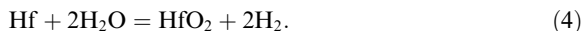
Assuming that all the oxygen from the dissociation of water in Eq. (4) reacts with hafnium to form a uniform, adherent, stoichiometric, non-porous oxide layer, the oxide film thickness can be estimated from the weight gain of the corrosion specimen. [2]

During the course of each test, periodic weight change measurements were recorded. It was from such

data that the correlations described in this paper were obtained. Fig. 1(a)–(c), which represent tests 1, 11 and 19 (as identified in Table 2), illustrate the corrosion behavior that was typically observed at all temperatures in both autoclave and ATR test environments. As exemplified by Fig. 1(c), the corrosion of unalloyed hafnium displays three distinct kinetic regimes, and two distinct transition points. These regimes and transition points are schematically illustrated in Fig. 2 and are described as follows:

1. During the first regime, the oxide film weight-gain rate decreases with exposure. This suggests that the oxide film serves as a protective adherent barrier to the further corrosion of the hafnium metal substrate. Visually, the corrosion coupons exhibit a multicolored, iridescent, semitransparent film in the early stage of exposure. The color changes to a lustrous black in the later stage. The oxide film in this regime grows approximately in accordance with a cubic rate relationship. The regime is referred to as the pretransition regime.

---

[2] 14.7 mg/dm² of weight gain = 1 μm of oxide growth = 0.6 μm of metal consumed.
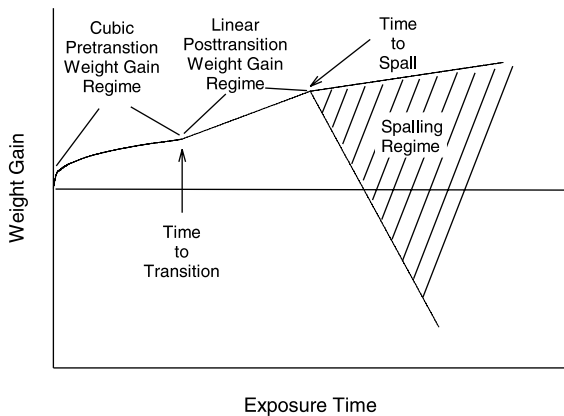
Fig. 2. Schematic illustration of the three hafnium corrosion regimes and two transition points.

2. The pretransition and post-transition regimes are separated by the first transition point, or what will be referred to as the time-to-transition (TTT).

3. In the post-transition regime the corrosion kinetics are best described as linear. That is, the corrosion rate is constant. The oxide film exhibits a combination iridescent, semigloss light gray finish.

4. The post-transition and oxide spalling regimes are separated by the second transition point, or what will be referred to as the time-to-spall.

5. The spalling regime is characterized by weight loss and a significant amount of weight-change variability. The corrosion film in this regime exhibits a matte gray appearance and is powdery and can be removed with minimal effort. In this regime small levels of spalling can result in relatively large changes in weight change. This is because adherent corrosion involves only the uptake of oxygen, whereas spalling involves the loss of both oxygen and hafnium (in the form of HfO_2), with hafnium being much heavier than oxygen. For example, a weight loss of 10 mg/dm^2 from a sample that had a corrosion weight gain of 10 mg/dm^2 would require only 15 percent of the oxide film to have spalled from the surface. Scanning electron microscopy has shown that hafnium spalling involves loss of microfine particles of crystalline oxide film that fractures from the surface.

With the exception of the magnitude of the weight gains being less, the corrosion behavior of hafnium in high-temperature water between the temperatures of 260–360 °C is very similar to that of crystal-bar zirconium [12]. In early stages of exposure, crystal-bar zirconium develops a lustrous black, tightly adherent corrosion film. At some point during the exposure, a rapid increase in the corrosion kinetics is observed with

crystal-bar zirconium, coincident with the formation of a white corrosion product, which is followed shortly by the loss of oxide through spalling.

3.2. Method of data analysis

Some samples had oxide films, i.e., prefilms, at the start of the tests and some did not. To take into account the effect of prefilming, adjustments were made to the specimen exposure times. This was done to effectively reference the start of each test at time, $t = 0$. Using an initial estimate of the pretransition corrosion rates, which were later refined by iteration, the number of equivalent days of exposure at any given test temperature was calculated from the average prefilm weight. For specimens in which no prefilms were applied, no adjustments were made to their exposure times.

The corrosion kinetic data obtained from each of the tests were analyzed to determine best-fit correlations in both the pretransition and post-transition corrosion regimes. In addition, the times to the first transition (TTT) were correlated as a function of temperature. The analyses were conducted using a variety of software packages. The SOLO statistical software package was used to determine the delineation between the pretransition and post-transition regimes, i.e., the TTT. To determine the best-fit correlations of corrosion weight gain as a function of exposure time, standard linear regression techniques were used. In each of the tests identified in Table 2, correlated fits were made through the averaged weight gain data for each time interval. The pretransition correlations were made on measurements obtained prior to the TTT, whereas the post-transition correlations were made on measurements obtained between the time to transition and the onset of spalling as indicated by weight losses. The method by which the time to transition, which delineates the pretransition and post-transition corrosion regimes, was obtained is described below.

In general, at any given temperature, the kinetics of corrosion can be described by the empirical equation $\Delta W^n = kt$, where ΔW is the weight gain per unit area of the original surface in units of mg/dm^2, t is the exposure time in days, and n and k are constants for a given temperature [13]. When n is equal to 3, the rate equations are said to be cubic; when n is equal to 2, the rate equation is said to be parabolic, and when n is unity, linear kinetics occur. In the last case, the oxidation process is considered to be nonprotective. As the protective nature of the oxide increases, the value of the exponent n increases. In the correlations described below, only corrosion-kinetic data that are in the pretransition and post-transition corrosion regimes are evaluated. Data that are within the spalling regime are excluded from the analysis.

3.2.1. Pretransition correlations

The pretransition corrosion kinetics at a given temperature are approximated by the general equation $\Delta W = k_{c''} t^{1/n}$, where $k_{c''}$ is an empirical constant, which is termed the pretransition rate constant, and n is a constant that is greater than or equal to 2. The constants of the applicable rate equations are determined by using the logarithmic form, $\log \Delta W = \log k_{c''} + 1/n \log t$. A plot of ΔW against time t on logarithmic coordinates yields a straight line having a slope of $1/n$.

Values of $k_{c''}$ and $1/n$ are determined for each test from the data that are within the pretransition regime. The values of the best fit pretransition rate constants, $k_{c''}$, and exponents n, along with the times to transition are listed in Table 3. The exponents n ranged from 2.60 to 3.63, averaged 3.08, and did not appear to be a function of temperature. In developing a correlation to be used for engineering purposes, it is assumed that the exponent is a constant, and that the best fit is a cubic correlation, (i.e., $n = 3$), for each of the tests evaluated. Based on a value of n equal to 3, each of the coefficients $k_{c''}$ were normalized. This normalization was done by forcing the correlation for each test to fit through the averaged coupon weight gain at the last examination time in the pretransition regime. The resulting normalized coefficients, $k_{c'}$, also are listed in Table 3.

The corrosion-kinetic variation with temperature is modeled as a multiplier, i.e., rate constant to the time variable. The resulting equation, as a function of temperature, is of the form $k_c = A_c e^{-Q_c/T}$. The values of A_c and Q_c are determined by a least squares linear regression analysis, Fig. 3, of the natural logarithm of the cube, of $k_{c'}$ (i.e., $(k_{c'})^3 = k_c$), of the pretransition hafnium corrosion rate constants (from each test) vs. inverse temperature (K), (weighted by the number of corrosion coupons). The resultant correlations obtained are

$$\Delta W^3 = \left(5.65 \times 10^{12}\right) \exp\left(\frac{-17\,883 \pm 995}{T}\right) t \left(\frac{\text{mg}}{\text{dm}^2}\right)^3,$$
(5)

$$\Delta W = \left(1.78 \times 10^4\right) \exp\left(\frac{-5961 \pm 332}{T}\right) t^{1/3} \left(\frac{\text{mg}}{\text{dm}^2}\right),$$
(6)

Table 3
Summary of pretransition correlation constants and TTT

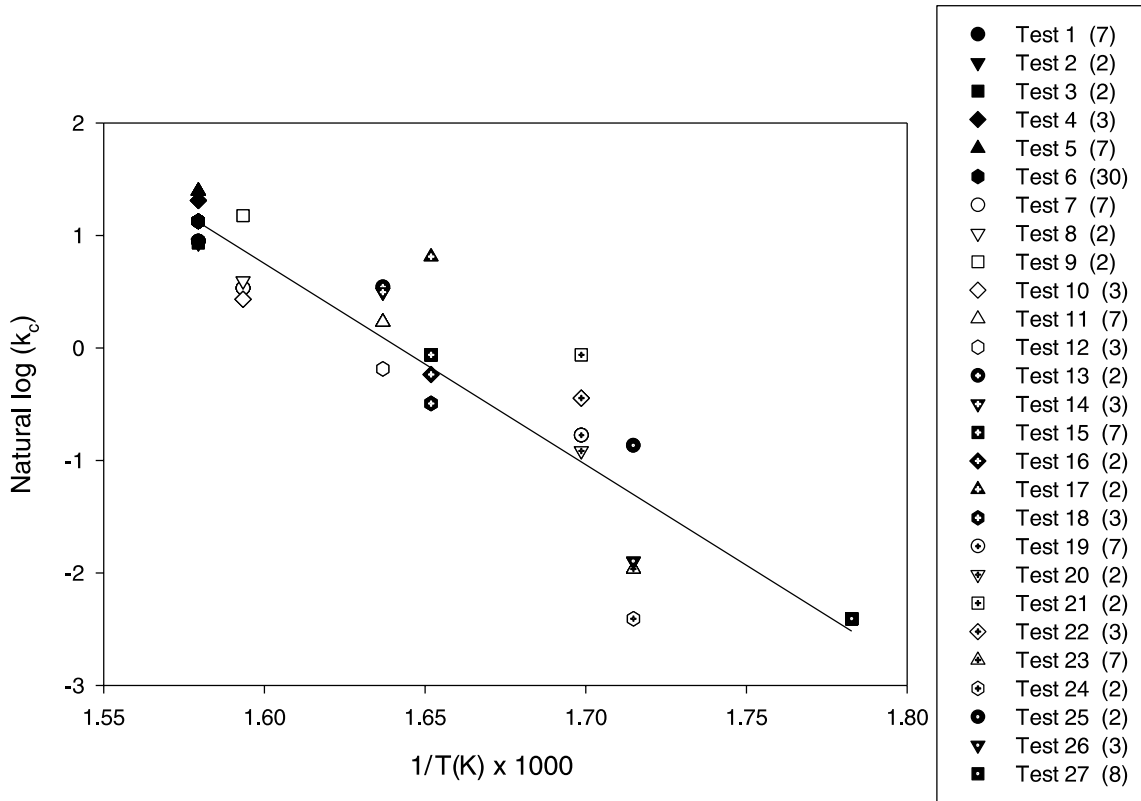| Test	Group	Pretransition constants		Temp. (°C)	Time to transition (days)	Time of last avg. weight gain (days)	Normalized pretransition constants, $k_{c'}$ (with $n = 3$) (mg/dm²/day)	k_c (= $(k_{c'})^3$) (mg/dm²/ day)³
		$k_{c''}$	n'					
1	A	1.42	3.06	360	189	185	1.37	2.57
2		1.42	3.07			196	1.36	2.52
3		1.42	3.07			196	1.36	2.52
4		1.53	2.98			182	1.55	3.72
5	B	1.55	2.95	360	193	112	1.59	4.02
6	C	1.67	3.26	360	180	180	1.45	3.05
7	D	1.49	3.44	354	212	183	1.19	1.69
8		1.51	3.42			186	1.22	1.82
9		1.69	3.25			178	1.48	3.24
10		1.47	3.49			176	1.15	1.52
11	E	1.08	3.00	338	409	368	1.08	1.26
12		1.00	3.10			366	0.94	0.83
13		1.15	2.94			374	1.20	1.73
14		1.14	2.95			364	1.18	1.64
15	F	0.84	2.77	332	396	249	0.98	0.94
16		0.81	2.8			252	0.92	0.78
17		0.99	2.6			238	1.31	2.25
18		0.77	2.86			396	0.85	0.61
19	G	0.70	2.88	316	1291	1200	0.77	0.46
20		0.68	2.90			1207	0.74	0.41
21		0.82	2.79			1178	0.98	0.94
22		0.75	2.83			1141	0.86	0.64
23	H	0.72	3.50	310	1473	1169	0.51	0.13
24		0.67	3.63			1218	0.44	0.09
25		0.87	3.21			1148	0.75	0.42
26		0.70	3.41			1102	0.53	0.15
27	I	0.42	2.95	288	4100	4098	0.44	0.09

Fig. 3. Natural logarithm of the pretransition hafnium corrosion rate constant, k_c, vs. 1/Temperature (K). The number in parentheses in the legend indicates the number of corrosion coupons included in the correlation.

From Eq. (5) an activation energy, Q, of 148.3 kJ/mol is obtained.

3.2.2. post-transition correlations

Data in the post-transition corrosion regime are described by linear corrosion kinetics. That is, $\Delta W = k_L t$, where k_L is in units of mg/dm^2/day and is termed the linear rate constant. Values of k_L are determined from each test, (with the exception of Tests Nos. 6, and 23, 24, 25 and 26, in which insufficient data exist to support estimating k_L, for the post-transition correlation), and are listed in Table 4. As is the case for the pretransition corrosion regime, the corrosion kinetic variation with temperature is modeled as a multiplier to the time variable, i.e., $k_L = A_L e^{-Q_L/T}$. In Fig. 4 the natural logarithm of the linear rate constant vs. inverse temperature (K) is plotted. Based on a linear regression analysis, the following correlation is obtained:

$$\Delta W = \left(2.00 \times 10^6\right) \exp\left(\frac{-11133 \pm 860}{T}\right) t \left(\frac{\text{mg}}{\text{dm}^2}\right). \tag{7}$$

From Eq. (7), an activation energy of 92.6 kJ/mol is derived.

3.2.3. Time-to-transition

As shown above, the corrosion of hafnium is characterized by the initial formation of a thin, iridescent, tightly adherent oxide film, corresponding to an approximately cubic rate relationship behavior up to a weight gain of 7 mg/dm^2 to 10 mg/dm^2 (0.5 μm to 0.7 μm of oxide). Further exposure beyond this point produces linear kinetics. The point on the corrosion weight gain curve where the cubic and linear portions of the corrosion kinetics curve intersect is termed 'transition' [12]. In determining the TTT, use was made of the fact that, at any given temperature and pH, the tests listed in Table 2 were conducted in the same autoclave or ATR loop. Thus, the tests described in Table 2 were categorized into groups. For each group, [3] the averaged weight gain vs. time data (for each of the tests within that group) were analyzed using the SOLO statistical software

---

[3] For any test within a given test group, the materials were obtained from the same ingot and exposed under the same conditions, i.e., temperature and pH. The only difference between each of the tests within any given test group was in the oxide prefilms that had been applied prior to testing.

Table 4
Summary of post-transition correlation constants

Test	Temperature (°C)	post-transition rate constants, k_L (mg/dm^2/day)
1	360	0.05042
2		0.04170
3		0.04170
4		0.05173
5		0.03878
6		[a]
7	354	0.03151
8		0.02622
9		0.03372
10		0.03517
11	338	0.02552
12		0.02753
13		0.01831
14		0.02358
15	332	0.02440
16		0.02414
17		0.02825
18		0.02517
19	316	0.01675
20		0.01675
21		0.02440
22		0.01022
23	310	[a]
24		
25		
26		
27	288	0.00327

[a] Insufficient data to establish trend.

package. From this method of grouping and analysis, the TTT data listed in Table 3 were obtained.

A plot of the natural log of the time to transition values, as listed in Table 3, versus inverse temperature is shown in Fig. 5. The expression for the time to transition correlation plotted in Fig. 5 is

$$\text{TTT} = \left(4.68 \times 10^{-9}\right) \exp\left(\frac{15415 \pm 1,494}{T}\right) \quad \text{(Days)}. \tag{8}$$

3.3. Metallography

To illustrate the nature of the oxide films that formed on hafnium in the pretransition, post-transition, and spalling regimes, corrosion coupons from each of these regimes were examined. The oxide films that were observed on these coupons are typical of oxide films that have been observed on Hf from over 25 years of testing. The corrosion coupons that were examined were removed from 360 °C, pH 7 autoclave tests. Scanning electron microscope (SEM) examinations of both the surface of the oxide layer and its cross-section were performed. Prior to examining the surface of the oxide layer a conductive gold coating was applied. The specimens were sectioned and mounted in a hot press. To enhance oxide film edge retention, an aluminum foil layer was wrapped around the specimen prior to mounting. The specimens were ground to remove approximately 500 µm of material on a Petrodisc-M wheel with a slurry comprised of 15 µm diamond abrasive and Struers DP-Green lubricant. Rough polishing was performed in two steps by first using a DP-Plan fine grinding nylon cloth with a 15-µm diamond suspension, which was then followed by a polish using a met cloth with 6-µm diamond paste. Final polishing was performed using a microcloth with Linde B and an acid polish solution consisting of 870 ml H_2O, 10 ml HF (49 wt% in water), 20 ml HNO_3 (70 wt%) and 100 gms Oxalic acid (98 wt%). The purpose of the acid polish solution was to prevent smearing of the metal during the final polishing step. To reveal the grain boundaries in the metal substrate, the specimens were swab etched using a solution comprised of 60 ml H_2O_2 (30 wt%), 30 ml HNO_3 (70 wt%), 30 ml ethanol and 2 drops of HF (49 wt%).

3.3.1. Pretransition oxide

A sample that had attained a final weight gain of 6.2 mg/dm^2, after 125 days at 360 °C, was removed from autoclave testing. This coupon was expected to exhibit cubic pre-transition corrosion kinetics since at 360 °C the predicted time to transition (per Eq. (8)) was 174 days. To the eye, the oxide exhibited red, blue, and green iridescence. The surface as seen with the SEM is shown in Fig. 6. The bulk of the oxide surface as seen in the planar SEM view is smooth and featureless. The smooth areas appear to be bounded by ridges of apparently thicker fractured oxide film. From the size and shape of the pattern produced, the network of cracks appears to follow grain boundaries in the original metal surface. No spalling is observed.

A cross-sectional view of the oxide formed is shown in Fig. 7. For the most part the oxide has a uniform thickness of approximately 0.4 µm; (Note: Based on Eq. (6), a weight gain of 7.33 mg/dm^2 and an oxide thickness of 0.50 µm would have been predicted.) However, there are instances where, in cross section, nodular-like features are observed. The oxide associated with these features protrudes above the surface of the uniform oxide and penetrates into the Hf substrate. The oxide associated with these nodule-like features is on the order of 1–2 µm thick. These local penetrations of oxide appear to correspond to the network of cracks and defects observed in the planar examination.

3.3.2. post-transition oxide

Another coupon was removed from autoclave testing after 540 days at 360 °C. It had attained a final weight
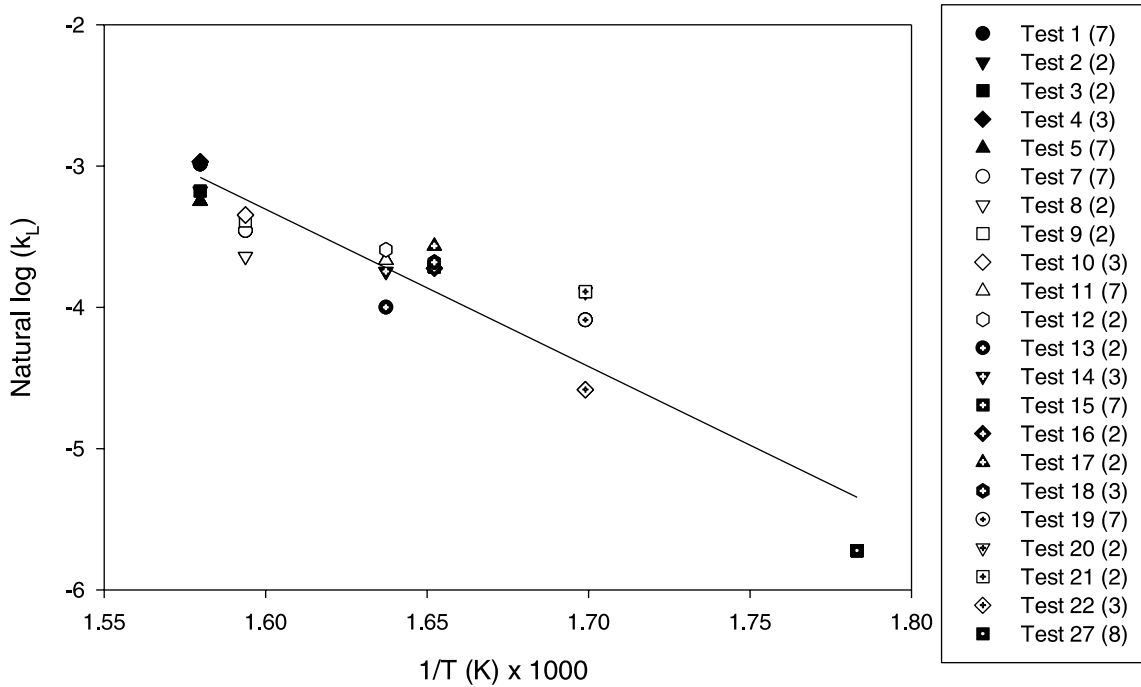
Fig. 4. Natural logarithm of the post-transition hafnium corrosion rate constant, k_L, vs. 1/Temperature (K). The number in parentheses in the legend indicates the number of corrosion coupons included in the correlation.
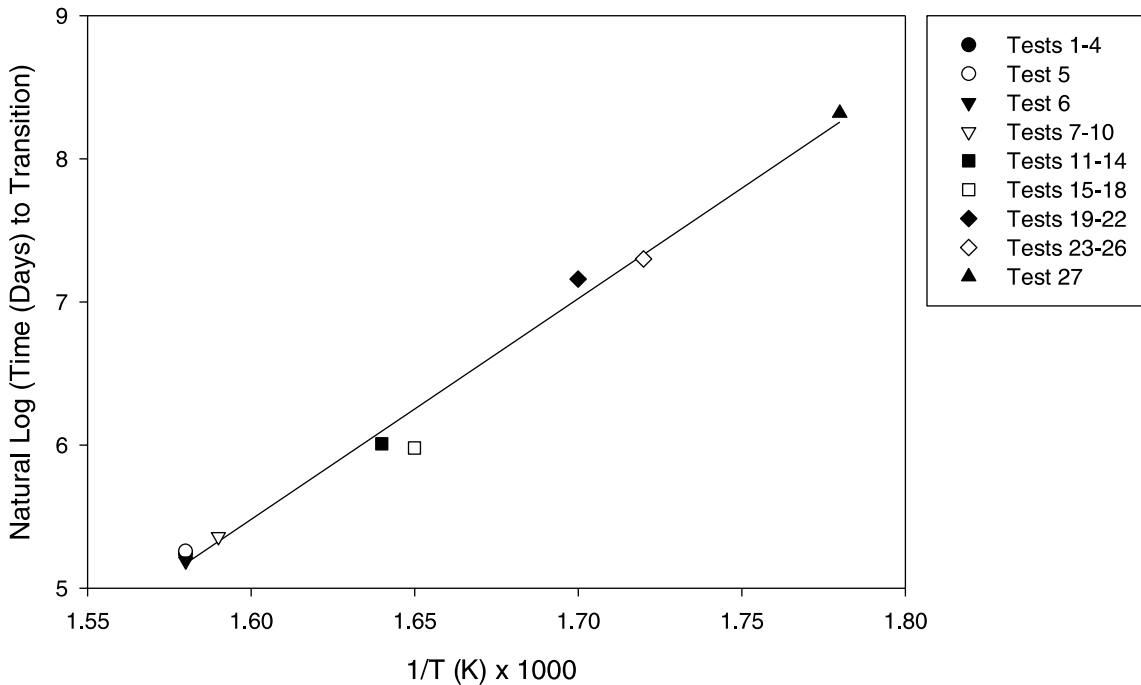

Fig. 5. TTT vs. $1/T$ (K).

gain of 15.1 mg/dm^2. This coupon was expected to exhibit linear post-transition corrosion kinetics. Visually,

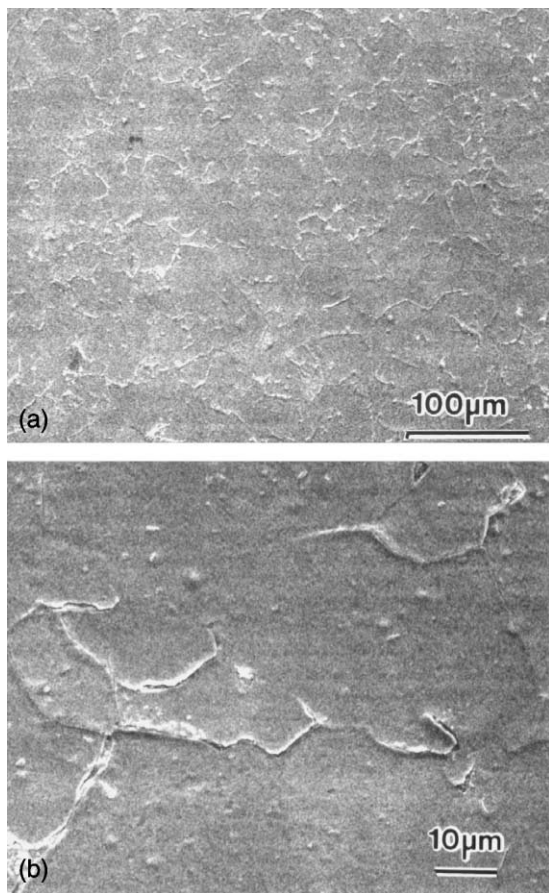the oxide surface was light gray in appearance with some evidence of iridescence. The surface SEM examination

Fig. 6. SEM micrographs of the surface of a pretransition oxide film as observed on a coupon that had been exposed in autoclave (pH 7) at 360 °C for 125 days. A 3-day 360 °C thermal prefilm had been applied prior to testing; (b) is a 5 × magnification of (a).

Fig. 7. SEM cross-sectional micrographs of the pretransition oxide; (a) example of the uniform, adherent oxide film, (b) example of a nodule-like oxide feature.

of this coupon, see Fig. 8, found that a network of defects existed, which were more pronounced than the cracks observed for the 125-day coupon shown in Figs. 6 and 7. The oxide along this network was rough and exhibited evidence of oxide spalling. Within the fractured network were islands of oxide that appeared relatively smooth. These areas are probably regions covered by a thin, uniform, adherent oxide.

As shown in Fig. 9, a cross-sectional SEM examination of this coupon found that for the most part this coupon is covered by an adherent corrosion film that was quite thin, measuring less than 1 μm in thickness. In addition to the thin adherent oxide, there were regions in which the nodular-like oxide existed. In contrast to the pretransition regime, the nodular-like features were observed to be both more frequent and had penetrated deeper (up to 5 μm) into the hafnium metal substrate. Relating the surface micrographs of Fig. 8 to the cross-

sectional micrographs of Fig. 9, the regions surrounded by the fractured network of oxide correspond to the thin adherent portion of the oxide film. On the other hand, the fractured network observed in Fig. 8 corresponds to the nonuniform fractured oxide layers observed in Fig. 9. Fig. 10 shows this coupon after having been etched to reveal the grain boundary structure. This micrograph illustrates that the nodule-like oxide features are correlated to the hafnium metal substrate grain boundaries.

3.3.3. Spalling oxide

A coupon that demonstrated oxide spalling is shown in Fig. 11. This coupon had been exposed for 731 days at 360 °C and exhibited a weight loss of 26.7 mg/dm^2. The oxide layer was off-white in color. Powdery white oxide was easily removed by rubbing. Micrographs of the surface oxide layer illustrate that the majority of the coupon surface is rough and uneven. However, within the rough regions there are islands of oxide which appear relatively smooth. It is likely that these regions
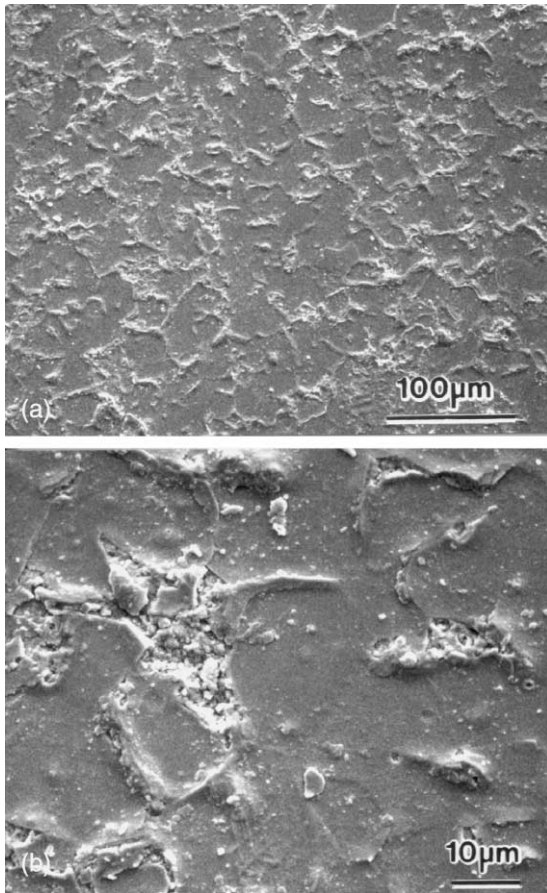
Fig. 8. SEM micrographs of the surface of a post-transition oxide film on a coupon that was exposed in autoclave testing (pH 7) at 360 °C for 540 days. No oxide prefilming was applied to the specimen prior to the test; (b) is a 5 × magnification of (a).
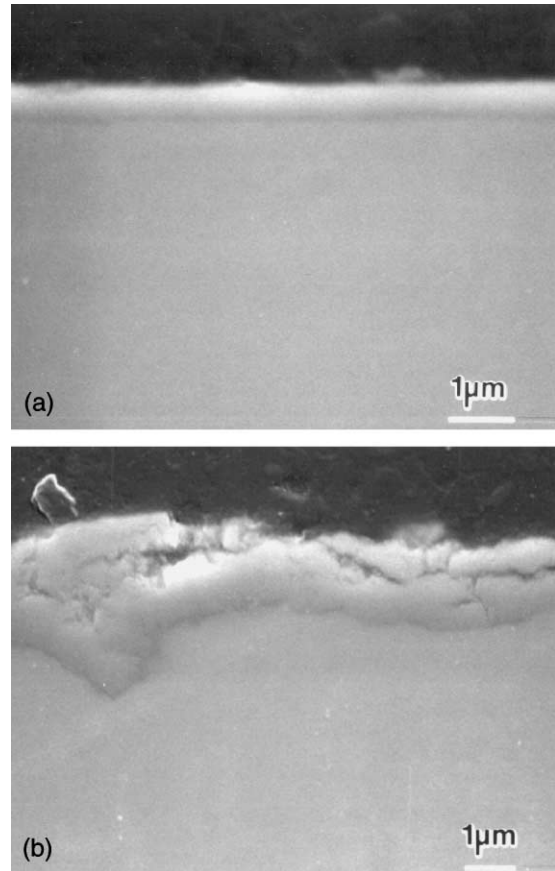

Fig. 9. SEM cross-sectional micrographs of the post-transition oxide film that existed on the same coupon shown in Fig. 8; (a) example of the uniform, adherent oxide film, (b) example of a nodule-like oxide feature.

correspond to portions of the oxide layer that are thin, uniform, and adherent.

In cross-section (Fig. 12) the majority of the coupon surface is seen to be covered by a fractured, multilayered oxide film, with each layer tending to be on the order of 1 μm or less. In addition, the layered structures of the oxide regions that exhibit spalling appear to be more loosely connected than those in oxides that do not appear to be spalling. This suggests that the layer boundaries are fracture planes for the spalling process.

In summary, the metallograhic examinations have ascertained that in the pretransition regime, where cubic corrosion kinetics are exhibited, a thin (<1 μm), adherent, protective oxide layer exists. The onset of the post-transition corrosion regime, where linear corrosion kinetics are observed, occurs as a result of the localized breakdown of the oxide film into a nodular-like oxide film. The breakdown of the oxide film is associated with

the hafnium metal grain boundaries. As the spalling regime is entered, the nodular-like features grow in size, both laterally along the oxide surface and in depth into the metal substrate (Fig. 13). Their growth corresponds to an increasing percentage of the total specimen surface. Due to its friable nature, the oxide film is susceptible to a powdery form of spalling, and weight losses occur.

3.4. Hf vs. Zircaloy corrosion rate comparison

The corrosion rate of hafnium is less than that for Zircaloys. With the use of Eqs. (6)–(8), this difference in corrosion performance can be quantified. Use was made of the relationships presented by Hillner in Ref. [12] in comparing the pretransition, post-transition and TTT behavior. The ratios of the relevant Hf to Zircaloy rate equations are summarized in Table 5 for two temperatures, 100 and 310 °C. The data in this table illustrate that in both the pretransition and post-transition
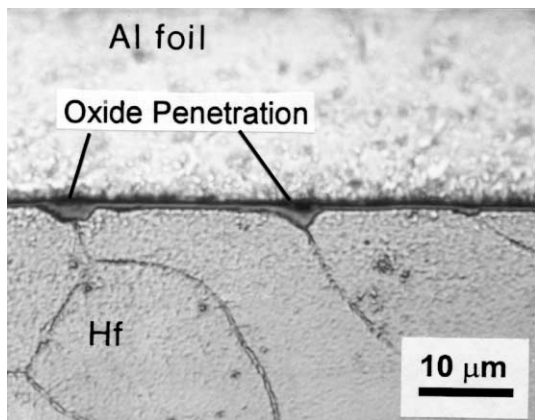
Fig. 10. Optical micrograph of the post-transition of the coupon shown in Figs. 8 and 9 (after etching) illustrating the nodule-like oxide features that penetrate along the hafnium metal grain boundaries.
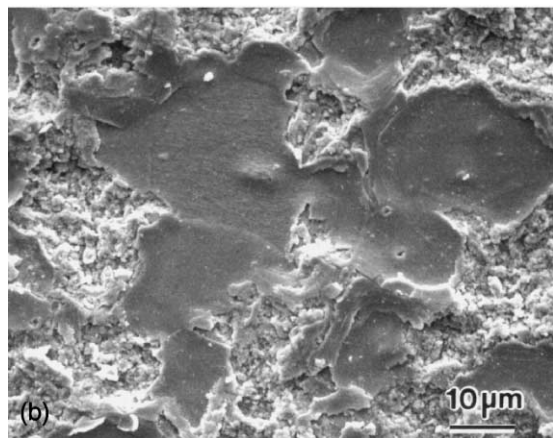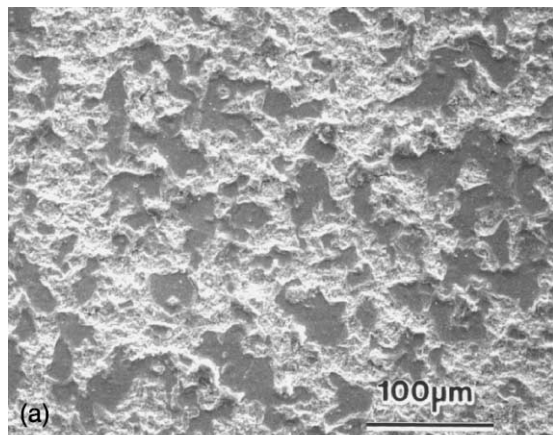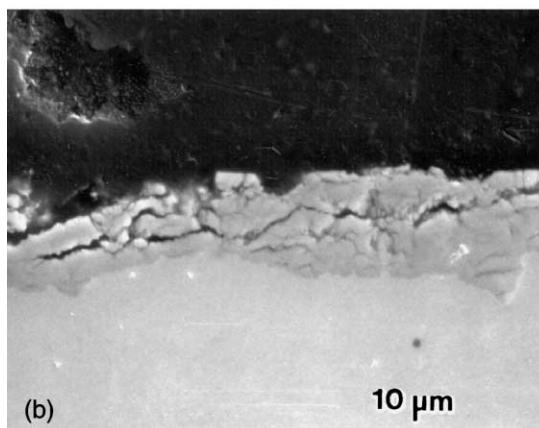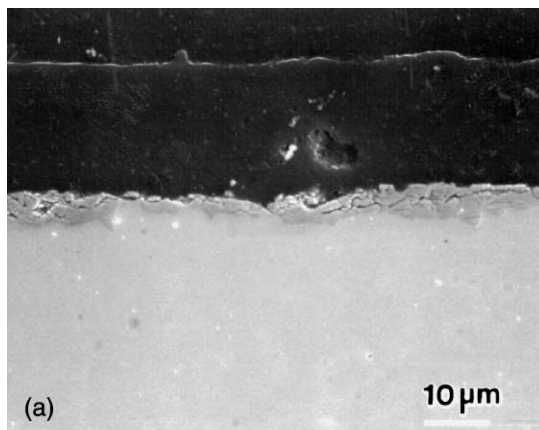

Fig. 12. SEM cross-sectional micrographs of the spalling regime oxide film shown in Fig. 13; (b) is a 3× magnification of (a).

Fig. 11. SEM micrographs of the surface of a spalling regime oxide film on a coupon that had been exposed in autoclave testing (pH 7) at 360 °C for 731 days. No oxide prefilming was applied to the specimen prior to the test; (b) is a 5× magnification of (a).

corrosion regimes, the corrosion resistance of hafnium is significantly greater than that of Zircaloy. In addition, the TTT of hafnium is longer than that for Zircaloy, e.g., at least 2.5 times greater at 310 °C, and increases as temperature decreases.

3.5. Influence of irradiation on corrosion

Comparisons of the in-reactor corrosion behavior of the Zircaloys with the out-of-reactor or ex-reactor corrosion behavior show that corrosion is enhanced by neutron irradiation [14]. For hafnium, data that show the effect of irradiation on corrosion behavior are more limited. Irradiation is expected to affect the corrosion behavior of hafnium in two ways. First, the corrosion product film, when subjected to a neutron flux, is expected to receive some form of radiation damage that could enhance corrosion. Second, due to its large neutron absorption cross-section, the resulting transmutation products of hafnium may affect its corrosion
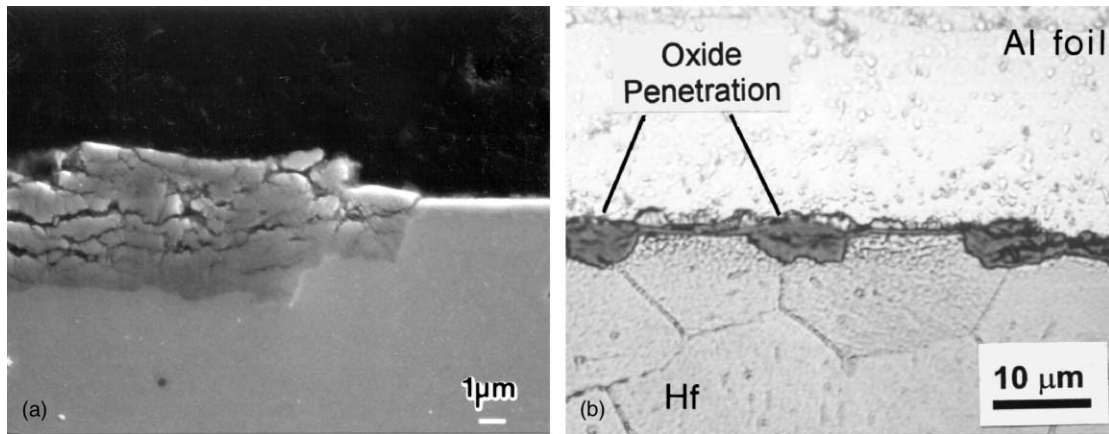
Fig. 13. Spalling regime on the coupon shown in Figs. 11 and 12, illustrating the growth of nodule-like oxide features.

Table 5
Ratios of the Hf-to-Zircaloy, pretransition and post-transition corrosion rate constants and the TTT at 100 and 310 °C

Temperature (°C)	Ratio of the Hf-to-Zr pretransition rate constants[a]	Ratio of the Hf-to-Zr post-transition rate constants[b]	Ratio of the Hf-to-Zr TTT[c]
100	0.05	0.75	76.7
310	0.18	0.20	2.55

[a] Ratio of Eq. (6) to the cube root of Eq. (3), Ref. [12].
[b] Ratio of Eq. (7) to Eq. (4), Ref. [12].
[c] Ratio of Eq. (8) to Eq. (6), Ref. [12].

behavior. Naturally occurring hafnium is composed of six stable isotopes: ^{174}Hf, ^{176}Hf, ^{177}Hf, ^{178}Hf, ^{179}Hf and ^{180}Hf. Tantalum, a major transmutation product is formed via the (n, γ) reaction of ^{180}Hf followed by the β^- decay of ^{181}Hf to the stable ^{181}Ta isotope. Tungsten and lutetium also are produced, but in much smaller quantities. For the control rod exposed during three seed lives in PWR Core 1 [11], tantalum and lutetium analyses were performed as a function of depth below the surface in regions that had been subjected to a radially (as referenced from the core center) averaged thermal neutron fluence of 4.17×10^{24} to 11.6×10^{24} n/m^2 (the radially averaged fast fluence (>1 MeV) ranged from 37×10^{24}

to 54×10^{24} n/m^2). This analysis showed that the tantalum and lutetium concentrations are, in general, higher near the material surface and are proportional to neutron fluence (Table 6).

Due to the confounding effect of neutron absorption on corrosion weight gain measurements, the impact of irradiation on corrosion can only be ascertained through oxide thickness measurements, as obtained via destructive examination. Thus the amount of data available is more limited as compared to weight change data. In-reactor data that have been obtained through destructive metallographic examinations are presented in Table 7. In this table the average metallographically measured

Table 6
Tantalum and Lutetium analyses (wt%) [11]

Specimen number	Thermal neutron fluence ($\times 10^{24}$ n/m^2)	Surface		127 μm depth		254 μm depth		381 μm depth		635 μm depth	
		Ta	Lu	Ta	Lu	Ta	Lu	Ta	Lu	Ta	Lu
G-3–10	11.60	1.02	0.05	0.72	0.04	0.65	0.04	0.67	0.05	0.55	0.05
G-3–9	7.61	0.65	0.04	0.47	0.04	0.36	0.03	0.38	0.03	0.27	0.03
G-3–8	6.16	0.57	0.03	0.36	0.03	0.33	0.03	0.31	0.03	0.24	0.03
N-3–9	5.15	0.40	0.02	0.29	0.03	0.26	0.02	0.22	0.02	0.20	0.02
N-3–8	4.17	0.34	0.02	0.29	0.02	0.24	0.02	0.19	0.02	0.17	0.02

Table 7
Comparison of measured and predicted oxide thicknesses for Hafnium exposed under irradiated conditions

Sample	Temperature (°C)	Exposure time (Days)	Fast neutron fluence ($\times 10^{24}$ n/m^2)	Average measured oxide thickness (μm)	Range of oxide thicknesses calculated by Eq. (6) (μm)
1[a]	280	1100	4.17–11.60	0.27[b]	0.14–0.48
2	310	1903	190.8	0.64[c]	0.31–0.96
3	285	2749	55	<1.0[d]	0.22–0.71
4	298	765	83	<1.0[d]	0.18–0.58
5	254	3442	76	<0.5[d]	0.12–0.42

[a] From the Shippingport PWR core 1 control rod [11].
[b] Measured via X-Ray absorption technique.
[c] Measured via SEM.
[d] Less than the resolution of the hot-cell optical microscope.

oxide thickness is compared with the range of oxide thicknesses as predicted by the out-of-pile pretransition weight gain correlation, Eq. (6).

The following conclusions are drawn from these comparisons. First, the in-flux measured oxide thicknesses fall within the expected range of values predicted for pretransition corrosion kinetics, as correlated from the autoclave and out-of-flux studies; therefore, it is concluded that corrosion is not accelerated by irradiation. Second, the increase in tantalum buildup has no effect upon the corrosion rate. Based on these observations, it is expected postirradiated corrosion within the pretransition regime would be unaffected by prior irradiation. Data that would illustrate the effect of irradiation on post-transition corrosion behavior are not available.

4. Conclusion

High-temperature water corrosion data for hafnium has been evaluated. Hafnium is observed to exhibit pretransition, post-transition, and spalling corrosion regimes. For the pretransition and post-transition regimes, correlations are developed that are functions of time and temperature. For the pretransition regime, cubic corrosion kinetics are observed, whereas in the post-transition regime, linear corrosion kinetics are observed. The data show that for the pretransition and post-transition regimes, hafnium is more corrosion resistant than zirconium or the Zircaloys. Metallography has determined that a thin, protective oxide layer is formed during the pretransition regime. The onset of the post-transition regime and the progression into the spalling regime are associated with the breakdown and loss of the oxide film from regions at hafnium metal grain boundaries. The correlations that are derived may be used as a basis for estimating the amount of corrosion that occurs on hafnium stored in a repository.

Neutron irradiation does not adversely affect the corrosion performance of hafnium.

References

[1] E. Hillner, D.G. Franklin, J.D. Smee, The corrosion of Zircaloy-clad fuel assemblies in a geologic repository environment, WAPD-T-3173, September 3, 1997.
[2] J.P. Pemsler, J. Electrochem. Soc. 111 (1958) 1067.
[3] J.P. Pemsler, J. Electrochem. Soc. 111 (1964) 1185.
[4] J.D. Gadd, E.B. Evans, Corrosion 17 (1961) 109.
[5] W.W. Smeltzer, M.T. Simnad, Acta. Met. 5 (1957) 328.
[6] N. Birks, G.H. Meier, in: Introduction to High Temperature Oxidation of Metals, Edward Arnold, London, 1983, p. 41.
[7] P. Kofstad, in: High Temperature Corrosion, Elsevier Applied Science, New York, 1988, p. 278.
[8] V.M. Chernishov, I.N. Vasilchenko, Control members of WWER-440 and WWER-1000 Power Reactors, Proceedings, IAEA Technical Committee Meeting on Advances in Control Assembly Materials for Water Reactors, International Atomic Energy Agency, Vienna, IAEA-TECDOC-813, 1993, p. 105.
[9] H. Shirayanagi, T. Fukumoto, S. Shiga, Advanced control rods for Japanese BWR Plants, Proceedings, IAEA Technical Committee Meeting on Advances in Control Assembly Materials for Water Reactors, International Atomic

Energy Agency, Vienna, IAEA-TECDOC-813, 1993, p. 135.

[10] G.J. Salvaggio, F.A. Nichols, J.P. Bacca, Jr., Properties of a hafnium control rod after exposure during two seed lives in PWR core 1, WAPD-TM-337, November 1962.

[11] G.J. Salvaggio, J.G. Weinberg, S. Kass, K.J. Longua, Properties of a hafnium control rod after exposure during three seed lives in PWR core 1, USAEC Report WAPD-TM-457, US Atomic Energy Commission, Bettis Atomic Power Laboratory, June 1965.

[12] E. Hillner, in: A.L. Lowe, G.W. Parry (Eds.), Zirconium in the Nuclear Industry, ASTM STP 633, American Society for Testing and Materials, 1977, p. 211.

[13] E. Hillner, in: Zirconium and its Alloys, The Electrochemical Society, 1966, p. 132.

[14] H. Stehle, F. Garzarolli, A.M. Garde, P.G. Smerd, in: D.G. Franklin, R.B. Adamson (Eds.), Zirconium in the Nuclear Industry: Sixth International Symposium, ASTM STP 824, American Society for Testing and Materials, 1984, p. 483.